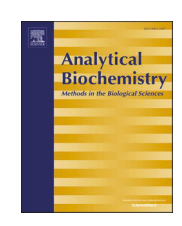
ELSEVIER

Contents lists available at ScienceDirect

Analytical Biochemistry

journal homepage: www.elsevier.com/locate/yabio





A novel ACE2-Based electrochemical biosensor for sensitive detection of SARS-CoV-2

Hamidreza Ghaedamini ^a, Khalid Khalaf ^b, Dong-Shik Kim ^a, Yuan Tang ^{b,*}

- ^a Department of Chemical Engineering, University of Toledo, USA
- ^b Department of Bioengineering, University of Toledo, USA

ARTICLE INFO

Keywords:
SARS-CoV-2
ACE2 enzyme
Aryl diazonium salt
Cyclic voltammetry (CV)
Electrochemical impedance spectroscopy (EIS)

ABSTRACT

SARS-CoV-2 emerged in late 2019 and quickly spread globally, resulting in significant morbidity, mortality, and socio-economic disruptions. As of now, collaborative global efforts in vaccination and the advent of novel diagnostic tools have considerably curbed the spread and impact of the virus in many regions. Despite this progress, the demand remains for low-cost, accurate, rapid and scalable diagnostic tools to reduce the influence of SARS-CoV-2. Herein, the angiotensin-converting enzyme 2 (ACE2), a receptor for SARS-CoV-2, was immobilized on two types of electrodes, a screen-printed gold electrode (SPGE) and a screen-printed carbon electrode (SPCE), to develop electrochemical biosensors for detecting SARS-CoV-2 with high sensitivity and selectivity. This was achieved by using 1H, 1H, 2H, 2H-perfluorodecanethiol (PFDT) and aryl diazonium salt serving as linkers for SPGEs and SPCEs, respectively. Once SARS-CoV-2 was anchored onto the ACE2, the interaction of the virus with the redox probe was analyzed using electrochemical impedance spectroscopy (EIS) and cyclic voltammetry (CV). Aryl diazonium salt was observed as a superior linker compared to PFDT due to its consistent performance in the modification of the SPCEs and effective ACE2 enzyme immobilization. A distinct pair of redox peaks in the cyclic voltammogram of the biosensor modified with aryl diazonium salt highlighted the redox reaction between the functional groups of SARS-CoV-2 and the redox probe. The sensor presented a linear relationship between the redox response and the logarithm of SARS-CoV-2 concentration, with a detection limit of 1.02×10^6 TCID50/mL (50% tissue culture infectious dose). Furthermore, the biosensor showed remarkable selectivity towards SARS-CoV-2 over H1N1virus.

1. Introduction

Human vulnerability to certain viral pathogens is well-documented, with their harmful impacts ranging from mild symptoms to severe pandemics resulting in high morbidity and mortality. As a consequence of the SARS-CoV-2 spread in 2020, the world witnessed not only the tragic loss of millions of lives but also profound disruptions in commerce, education, and general societal behavior. On March 11, 2020, the World Health Organization designated SARS-CoV-2 to be a pandemic after its rapid global spread. SARS-CoV-2 is a member of the broader coronavirus family. Respiratory droplets in the air and surfaces with intact virions are the main routes for the spread of the virus [1]. Diagnostics posed significant challenges during the pandemic, with the quantity of assays, expense of the necessary reagents, and time taken for results being major concerns. Although reliable tests for detecting the virus have been established, most of them necessitate prolonged

durations for the completion or rely on intricate and costly methods. The reverse transcription polymerase chain reaction (RT-PCR) is currently the most prevalent method for diagnosing COVID-19 [2]. The procedure entails collecting nasopharyngeal specimens with specific probes, transferring the viral content to a viral transport medium (VTM), and subsequently extracting its RNA [3]. While RT-PCR is a highly accurate technique, it has inherent limitations such as prolonged processing times, the necessity for specialized equipment, and the need for professional technicians. Turnaround times can range from several hours to multiple days. The financial burden associated with PCR tests poses challenges for widespread testing, particularly in resource-constrained regions [4]. Given these challenges, there is an urgent need for innovative diagnostic approaches that are not only accurate but also rapid, inexpensive, and easy to implement [5]. This has raised the focus on the research and development of electrochemical biosensors capable of detecting SARS-CoV-2 [6,7]. Electrochemical biosensors offer a

E-mail address: yuan.tang@utoledo.edu (Y. Tang).

^{*} Corresponding author.

potential pathway for the swift and precise identification of numerous pathogens and key clinical biomarkers [8]. A variety of electrochemical biosensors have been designed, functioning on diverse principles such as cyclic voltammetry (CV), linear sweep voltammetry (LSV), electrochemical impedance spectroscopy (EIS), and differential pulse voltammetry (DPV) [9–12].

For example, Olgac et al. used SARS-CoV-2 spike protein antibodies (S-AB) to develop two electrochemical biosensing platforms for the detection of SARS-CoV-2 spike protein antigen (S-AG) [13]. The first sensor, BSA/S-AB/GluAl/Cys/Au/GCE, involves electrodeposition of gold, chemisorption of cysteine, binding with glutaraldehyde, and immobilization of antibodies, finished with bovine serum albumin to cover open sites. The second sensor, BSA/S-AB/f-Cys/Au/GCE, diverges by using carbodiimide chemistry to activate carboxylic acid groups of cysteine, facilitating the covalent binding of the spike antibody to the activated cysteine surface. The sensors achieved detection limits of 0.93 ag/mL and 46.3 ag/mL, respectively [13]. Liv et el. developed electrochemical biosensors using functionalized graphene oxide modified glassy carbon electrode, which were further modified by immobilizing antibodies that are selective for either the wildtype or omicron proteins. The biosensors exhibited high sensitivity and selectivity in detecting the target proteins, with the detection limits reaching the ag/mL level [14]. Another interesting approach is to use SARS-CoV-2 spike antigen protein for the detection of SARS-CoV-2 spike antibodies. For example, an electrochemical biosensor for detecting SARS-CoV-2 spike antibodies was developed using gold clusters, cysteamine, and functionalized spike antigen protein [15]. The spike antigen protein was functionalized to create active sites that can form covalent linkages with the amine groups of cysteamine. The biosensor was successfully applied to detect antibodies spiked in real saliva and oropharyngeal swab samples, giving good recoveries [15]. On a related note, glutaraldehyde was used as a linker for the immobilization of SARS-CoV-2 spike antigen protein [16]. The sensor could detect the spike antibodies down to 0.01 ag/mL (ag/mL) in both synthetic samples and spiked saliva/swab samples [16]. In a different biosensor design, mercaptoethanol (CysOH) was used to immobilize the SARS-CoV-2 spike antigen protein [17]. In detail, CysOH molecules were chemisorbed onto gold clusters through their sulfur groups, exposing their hydroxyl groups on the surface. These hydroxyl groups then facilitated the binding of the SARS-CoV-2 virus spike gene through hydrogen bonding with its carbonyl/amino groups. This biosensor demonstrated remarkable sensitivity in detecting SARS-CoV-2 spike antibodies, achieving a detection limit down to 0.03 fg/mL [17]. These biosensing platforms focus on interactions between antibodies and antigens. While antigen-antibody interaction-based biosensors are widely used, they face limitations such as potential non-specific binding due to the constant region of antibodies, which can compromise specificity [18]. Additionally, these biosensors might not detect all virus strains effectively due to variations in antigens. In contrast, biosensors using the natural ACE2 receptor offer a significant advantage by directly targeting the SARS-CoV-2 spike protein, ensuring detection across all virus strains [1].

SARS-CoV-2 can attach to the angiotensin-converting enzyme 2 (ACE2) receptor on human cells, a process that enables it to infiltrate and start an infection [19]. This interaction is facilitated by the receptor-binding domain (RBD) of the spike (S) protein on the surface of SARS-CoV-2 virus, which interacts directly with ACE2 [20]. Multiple human tissues express the ACE2 receptor, including the lungs, heart, kidneys, and intestines [21]. The expression of ACE2 in these tissues may affect the severity and progression of COVID-19. The high ACE2 expression in the lungs and heart, for instance, may explain the severe respiratory and cardiovascular complications observed in some COVID-19 patients [21]. The interaction between the spike protein of the virus and the ACE2 receptor is crucial for the ability of the virus to infect host cells. This interaction is also pivotal in the development of therapeutic interventions. For instance, pharmaceuticals that inhibit the interaction between the spike protein and the ACE2 receptor could

prevent the virus from infecting and entering host cells. Vaccine development also requires an understanding of the interaction between SARS-CoV-2 and ACE2. Several vaccine candidates intend to stimulate an immune response against the spike protein, thereby inhibiting its ability to bind to ACE2 [22,23]. The spike protein of SARS-CoV-2 has a robust binding affinity to ACE2, characterized by a low nanomolar range, owing to the positive charge of the virus, in contrast to the negative charge of ACE2 [24,25]. This strong affinity paves the way for the application of ACE2 as a receptor in multiple biosensor designs. The hydrophobic domain of the ACE2 enzyme plays a critical role in its anchoring to cell membranes. This property permits the integration of ACE2 into fabricated amphiphobic structures resembling those of cell membranes. Furthermore, ACE2 has functional groups that can readily form covalent peptide bonds with certain compounds [26]. Notably, aryl diazonium salt, possessing carboxyl groups, can serve as a linker, establishing covalent bonds between its own carboxyl groups and the amine groups of ACE2.

For electrochemical biosensors to function optimally, surface functionalization and the chemistry of attachment are of paramount importance [27]. Gold surface-based sensors often rely on gold-thiol linkage for immobilizing biological molecules, particularly by establishing self-assembled monolayers (SAMs) on the gold surface [28]. SAMs may not only prevent non-specific adhesion of proteins, cells, and other elements from a sample medium to the electrode surface, but also ensure the proper orientation of biological sensing elements [29]. Self-assembled layers, including either a monolayer or complex multi-component structures, spontaneously form when gold surfaces come into contact with thiolated biomolecule solutions [30]. For carbon surface-based sensors, on the other hand, the immobilization of bio-recognition elements typically relies on techniques leveraging covalent bond formation [31].

Screen-printed electrodes (SPEs) have emerged as a promising platform in the field of electrochemical sensing, as they offer several advantages suitable for a broad range of applications [32]. The design versatility of SPEs is one of their most prominent features. They can be molded into a variety of shapes and sizes, making them suitable for many different applications [33]. SPEs have a substantial economic benefit since their manufacturing cost is far cheaper than that of many other electrode types, making them an enticing alternative for both the research and industrial sectors [34]. The flexibility of SPEs is further demonstrated by their adaptability to various surface modifications. These electrodes may be fine-tuned for a wide range of electrochemical analyses by integrating different metals, enzymes, complexing agents, or polymers [35–38]. Additionally, their disposability, user-friendliness, and swift response times strengthen their position as a preferred choice for efficient electrochemical sensing applications [39].

In the current study, two sets of electrochemical biosensors using a screen-printed gold electrode (SPGE) and a screen-printed carbon electrode (SPCE) are developed for detecting SARS-CoV-2 with high sensitivity and selectivity. The ACE2 enzyme, serving as a bioreceptor for the spike protein of the virus, was bound to SAMs immobilized on the electrode surfaces. First, a gold electrode was modified with a selfassembled monolayer (SAM) of 1H, 1H, 2H, 2H-perfluorodecanethiol (PFDT) which was subsequently bio-functionalized with the ACE2 enzyme. When PFDT is introduced to a gold surface, the thiol groups (-SH) of PFDT strongly adhere to the gold, forming a densely packed monolayer with the perfluorinated chains extending outward. Because the structure of the ACE2 enzyme includes hydrophobic tail regions that facilitate its entry into the cell membrane and given the amphiphobic nature of the PFDT SAM, the hydrophobic tail regions of ACE2 can be physiosorbed onto the fluorinated layer. Despite both the ACE2 enzyme and the PFDT surface being negatively charged, the primary interaction mechanism here is hydrophobic in nature. The hydrophobic interaction between the nonpolar regions of the ACE2 enzyme and the PFDT layer overcomes any electrostatic repulsion, allowing for efficient binding of the enzyme to the modified electrode surface [19,40,41]. In a separate set of experiments, the immobilization of ACE2 on the carbon electrode was achieved by modifying the SPCE using aryl diazonium salt, which acted as a linker to form the subsequent layer consisting of ACE2. The carboxylic end (-COOH) of the aryl diazonium salt binds with the amine group (-NH₂) of ACE2, resulting in a covalent peptide bond. Fig. 1 illustrates the fabrication processes and reaction mechanisms of the electrochemical biosensor.

2. Materials

Angiotensin-Converting Enzyme 2 (ACE2), 1H,1H,2H,2H-perfluorodecanethiol (PFDT), 2-(N-morpholino)-ethanesulfonic acid (MES), potassium ferricyanide K₃[Fe(CN)₆], potassium ferrocyanide, K₄[Fe (CN)₆]·3H₂O, 4-aminobenzoic acid (ABA), N-(3-dimethylaminopropyl)-N'-ethylcarbodiimide hydrochloride (EDC), N-hydroxysulfosuccinimide (NHS), hydrochloric acid (HCl), toluene, and sodium nitrite were acquired from Sigma-Aldrich (USA). Inactivated SARS-CoV-2 was obtained from ZeptoMetrix (USA). The virus was handled following the relevant biosafety-level protocols. Inactivated H1N1 virus was purchased from Microbiologics (USA). Pine Instruments in the USA supplied us with screen-printed electrodes of both carbon and gold types. Both types feature a working electrode with a 2 mm diameter, an auxiliary electrode, and a silver/silver chloride reference electrode. Electrochemical impedance spectroscopy (EIS) and cyclic voltammetry (CV) measurements were performed using a Gamry Reference 600 potentiostat from Gamry Instruments, USA.

2.1. Sensor preparation

Two different procedures were used to modify the electrodes, corresponding to the two types of electrodes used: SPGE and SPCE.

2.1.1. Modification of SPGEs using PFDT and ACE2 enzyme

A 1 mM solution of PFDT was achieved by adding PFDT to toluene while magnetically stirring, ensuring a uniform distribution of the PFDT. In a glass Petri dish, the SPGEs were placed horizontally, and 10 μ L of PFDT solution was dropped onto the working electrodes. The SPGEs were incubated at room temperature overnight, then cleansed with DI water and promptly dried with compressed air. The experiments with toluene were conducted under a safe fume hood, and the appropriate disposal methods for halogenated solvents were followed. Next, ACE2 was diluted from its stock concentration to 10 μ g/ml using DI water. Subsequently, a 10 μ L portion of the diluted ACE2 solution was applied to each working electrode on the SPGEs and incubated for 1 h at ambient temperature. After incubation, the SPGEs were washed with DI water and desiccated with compressed air [19,40].

2.1.2. Modification of SPCEs using aryl diazonium salt and ACE2 enzyme

A solution of aryl diazonium salt was achieved by adding 2 mM sodium nitrite to a mixture of 73 mM ABA and 1 mM aqueous HCl. The entire mixing process took place in an ice bath, where it was stirred for half an hour [42]. Aryl diazonium salt was electrochemically grafted onto the working electrode of the SPCE. This was achieved by immersing the working electrode in the solution of aryl diazonium salt and applying 15 consecutive cycles of CV in the potential range between 0 V and -1 V

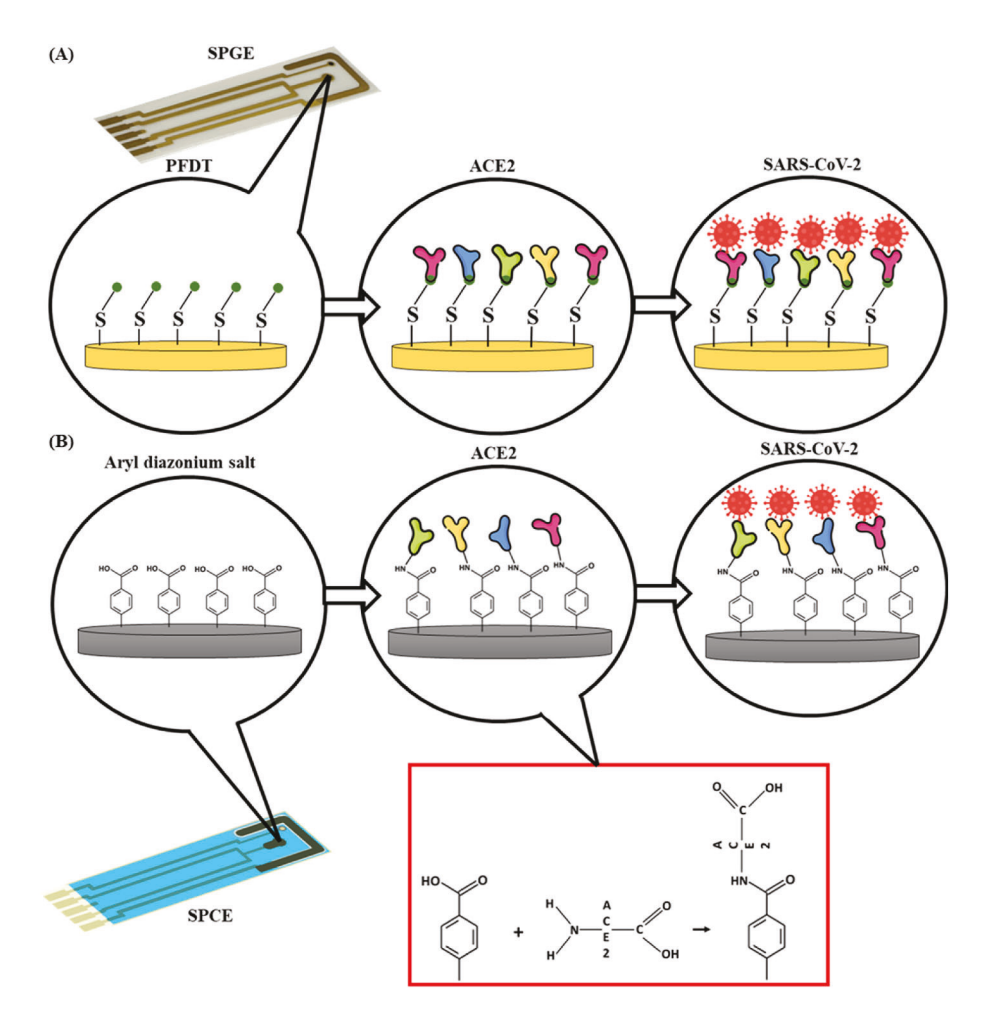


Fig. 1. Schematics illustrating the fabrication process of the electrochemical biosensors. (A) modification of SPGE with PFDT and the ACE2 enzyme. (B) modification of SPCE with aryl diazonium salt and the ACE2 enzyme.

at a scan rate of 200 mV/s. To remove weakly attached compounds, the treated electrodes were rinsed with DI water and methanol. Then, a 10 μL droplet of a 100 mM MES buffer solution with a pH of 4.5, containing 26 mM EDC and 35 mM NHS was deposited on the SPCE modified with aryl diazonium salt for 1 h to activate carboxylic entities on the electrode surface [43,44]. Finally, 10 μL ACE2 solution (10 $\mu g/ml$) was applied on the SPCE modified by aryl diazonium salt. An overnight incubation enabled ACE2 to covalently bond with the aryl diazonium on the surface of the electrode.

2.2. Capture of SARS-CoV-2 spike protein onto the electrochemical biosensors

Following the immobilization of the ACE2 enzyme, the SARS-CoV-2 virus was introduced to the modified electrodes. While the procedure was the same for both types of electrodes, the incubation time was different. 10 μL of the SARS-CoV-2 virus solution was drop-cast onto the surface of modified electrodes, with a 1-h incubation for SPGEs and a 12-h incubation for SPCEs.

2.3. The electrochemical measurements

At each step of modification, the electrochemical characteristics of the modified electrodes were assessed using EIS and CV in a 0.1 M phosphate buffer solution (pH = 7.2), with 5 mM [Fe(CN)₆]^{3-/4-} acting as the redox probe and 0.1 M KCl. The EIS measurements were performed over a frequency range of 0.1 Hz–100,000 Hz, applying an alternating current voltage of 5 mV. The direct current voltage was set at 0.23 V, which corresponds to the formal potential of the [Fe(CN)₆]^{3-/4-} redox couple. This specific voltage was chosen to ensure optimal conditions for accurate impedance measurements, as it represents the equilibrium point of the redox reactions involved [45]. The CV analyses were conducted in the potential range of -0.8 V to 0.8 V with a scan rate of 100 mV/s.

3. Results and discussion

3.1. Detection of SARS-CoV-2 using SPGEs modified with PFDT and ACE2

In Nyquist plots derived from EIS measurements, the linear segment observed at lower frequencies is indicative of a diffusion-limited

process, whereas a semicircular portion seen at higher frequencies signifies a charge transfer-limited process. Additionally, the diameter of the semicircle at these higher frequencies provides insight into the resistance of interfacial charge transfer (Rct) [42]. Fig. 2A shows the Nyquist plots of the SPGE at each step of functionalization. A notable trend of Rct increasing was observed with each step of modification. The Nyquist plot for the bare electrode, showing a very small, almost indistinct, semicircle, indicates a more efficient electron transfer process compared to electrodes modified with PFDT and ACE2, most likely due to the lack of insulating layers on the electrode surface [46]. Notably, upon the addition of the PFDT layer, there was a significant rise in R_{ct}, indicating that the PFDT layer impeded electron transfer. This impediment is attributed to the SAM nature of PFDT, which forms an insulating film on the surface of the electrode, thereby increasing the charge transfer resistance [47]. The subsequent addition of the ACE2 enzyme onto the PFDT layer resulted in a higher R_{ct}, confirming the successful immobilization of the ACE2 enzyme. This suggests that the enzyme introduced another insulating layer on the electrode surface, further inhibiting electron transfer [48]. Moreover, introducing the virus further increased the R_{ct}, highlighting the successful binding of SARS-CoV-2 to the ACE2 enzyme [40]. The EIS findings align with those of CV, where the bare electrode exhibits the highest current signal. The signal diminishes sequentially with the addition of PFDT, further with ACE2, and reaches its lowest when the virus is anchored to the ACE2 enzyme (Fig. 2B).

3.2. Detection of SARS-CoV-2 using SPCEs modified with aryl diazonium salt and ACE2

Fig. 3A illustrates the Nyquist plots of the bare electrode, the electrode modified with aryl diazonium salt, the electrode further modified with the ACE2 enzyme, and finally, the electrode with SARS-CoV-2. After the electrodeposition of aryl diazonium salt on the electrode, there was a significant rise in $R_{\rm ct}$ compared to the unmodified electrode. The increased diameter observed for the aryl diazonium-modified electrode is attributed to the organic salt layer on the electrode, which acts as a barrier to electron transfer, hence increasing the $R_{\rm ct}$ [49]. However, as the surface modifications continued, a reverse trend was observed. The semicircle diameter began to decrease with the subsequent modifications. First, the immobilization of the ACE2 enzyme onto the aryl diazonium layer resulted in a decreased diameter. The diameter was reduced even further when SARS-CoV-2 was bound to the ACE2 enzyme, which indicates a decrease in the charge transfer resistance.

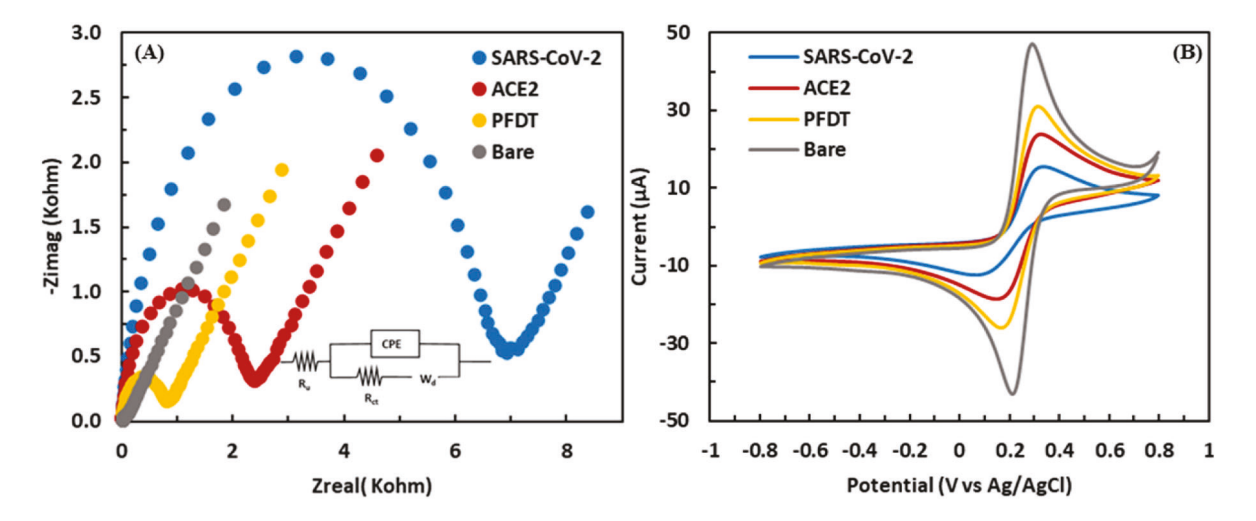


Fig. 2. Electrochemical characterizations of SPGE at each functionalization stage. (A) Nyquist plots showing increased R_{ct} with additions of PFDT, ACE2, and SARS-CoV-2 layers. The inset illustrates the equivalent electrical circuit. In this configuration, R_u signifies the resistance between the working and reference electrodes, R_{ct} represents charge transfer resistance, CPE stands for constant phase element, acting as a non-ideal capacitor, and W_d is a finite-length Warburg element indicative of ion diffusion. (B) Cyclic voltammograms with diminishing current signals through successive modifications.

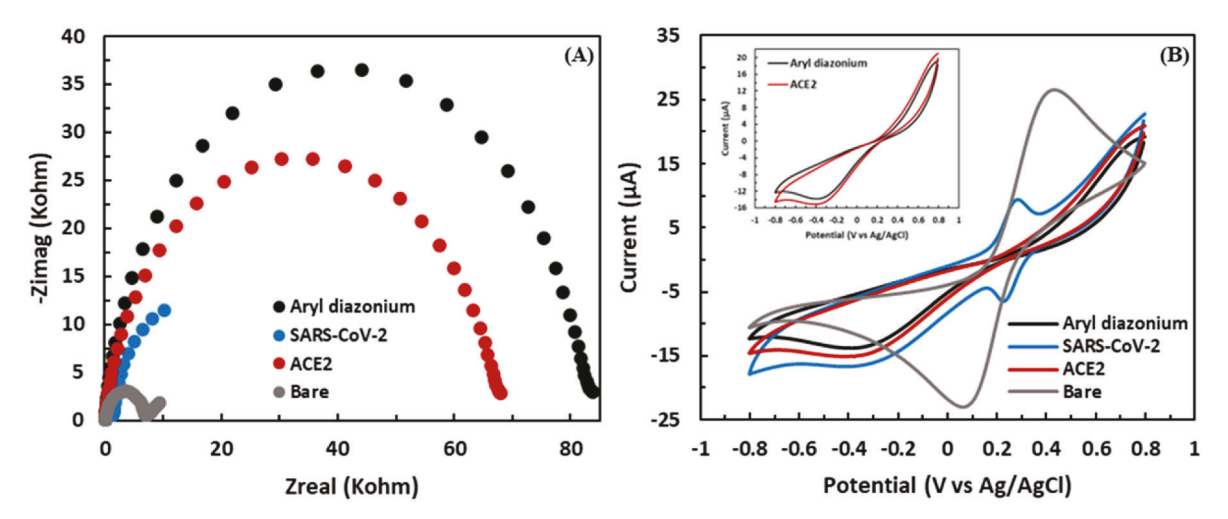


Fig. 3. Electrochemical characterizations of SPCE at each functionalization stage. (A) Nyquist plots showing the initial R_{ct} increase with aryl diazonium salt deposition on the bare electrode, followed by decreasing semicircle diameters with ACE2 enzyme immobilization and subsequent SARS-CoV-2 binding. (B) Cyclic voltammograms illustrating current variations at each step, with an inset providing a detailed view of the contrast between pre- and post-ACE2 immobilization.

Detailed analyses of the EIS fitting curves and deviations from these curves are presented in the Supplementary material, illustrating the application of the Constant Phase Element (CPE) with diffusion model across all steps of sensor modification.

CV analysis was additionally utilized to validate the effective electrodeposition of aryl diazonium salt, immobilization of ACE2 enzyme, and attachment of SARS-CoV-2, respectively. As seen in Fig. 3B, the curve corresponding to the bare electrode shows its current response to the redox probe, which declines significantly following the addition of aryl diazonium salt due to the high charge transfer resistance of aryl diazonium salt. However, after the immobilization of the ACE2 enzyme, there was a small increase in peak current in the cathodic region, i.e., a lowered charge resistance. This enhancement can be attributed to the intrinsic nature of the ACE2 enzyme, which is characterized by the presence of reactive functional groups [26]. These groups have the capacity to engage in redox reactions or charge transfer processes on the surface of the electrode, thereby enhancing electron transfer [50,51]. Following the binding of SARS-CoV-2 to the ACE2 enzyme, a distinct pair of redox peaks emerged in the cyclic voltammogram, likely due to the oxygenated functional groups of the virus taking part in the redox reaction [52].

The different trends observed in the Nyquist plots and cyclic voltammograms for the two electrode types could be attributed to the manner in which the ACE2 enzyme interacts with the PFDT layer and aryl diazonium salt, which affects the electron transfer process. If the enzyme molecule is oriented in a way that its reactive functional groups are used up for binding with the linkers, such as PFDT, the capacity of these groups to facilitate the transfer of electrons produced from the redox reaction between ACE2 and virus might be limited [44]. On the other hand, when diazonium salt was used as a linker, the reactive functional groups are thought to be unoccupied by the linker and remained active facilitating the charge transfer from the reaction between ACE2 and virus.

Through our investigation into identifying the most suitable linker for immobilizing the ACE2 enzyme, the application of PFDT as a linker presented significant challenges. Using PFDT to functionalize electrodes often resulted in inconsistent Nyquist plots and cyclic voltammograms. This could be attributed to the tendency of fluorocarbons, the primary components of PFDT, to form discrete phases by self-interaction, thus having limited miscibility in organic solvents [53–55]. This inconsistency in the PFDT modification process subsequently impacted the immobilization of the ACE2 enzyme and the capture of SARS-CoV-2, leading to further inconsistencies. In contrast, the carbon electrodes modified with aryl diazonium salt demonstrated remarkable

consistency. Given these observations, we opted to use aryl diazonium salt for the immobilization of the ACE2 enzyme in subsequent experiments.

3.3. Optimal SARS-CoV-2 incubation time

The optimal incubation time for the SARS-CoV-2 was investigated using CV analysis. As shown in Fig. 4, the cyclic voltammogram reveals no redox peaks with a 3-h incubation time. However, extending the incubation to 12 h enhances the redox response, due to the extended interaction of SARS-CoV-2 with the anchored ACE2 enzyme. However, extending the incubation time to 20 h did not significantly alter the redox peaks, possibly due to saturation of the ACE2 enzyme with SARS-CoV-2 molecules. Hence, the optimum incubation time for SARS-CoV-2 was determined to be 12 h.

3.4. Calibration curve

The response of the biosensor to different concentrations of SARS-CoV-2 ranging from 1.02×10^5 TCID50/mL to 1.02×10^8 TCID50/mL was assessed using CV analysis. TCID50/mL stands for 50% tissue culture infectious dose per milliliter indicating the viral titer at which 50% of the wells are infected and form viral plaques [56]. As shown in Fig. 5A, the redox response intensifies with increasing the concentration of SARS-CoV-2. Moreover, there is no clear redox peaks associated with the concentration of 1000-fold diluted SARS-CoV-2 (1.02 \times 10^5 TCID50/mL), likely due to the insufficient number of functional groups necessary for a discernible response. The redox response as specified in terms of electric current difference, ΔA , of the sensor was measured using the oxidation and reduction responses displayed in the cyclic voltammogram [57]. The biosensor illustrates a linear correlation between the redox response (ΔA) and the logarithm of the SARS-CoV-2 concentration within the range of 1.02 \times 10⁶ TCID50/mL to 1.02 \times 10^8 TCID50/mL, given by the equation $\Delta A = 5.59$ LogC - 30.07, $R^2 =$ 0.98 (Fig. 5B). The limit of detection (LOD) for SARS-CoV-2 was determined to be 1.02×10^6 TCID50/mL (concentrations below this threshold fail to produce a discernible change in the redox response of the biosensor [58]), demonstrating remarkable sensitivity of the biosensor.

3.5. Electrochemical reaction kinetics

The kinetics of the electrochemical reaction was examined by incrementally changing the scan rate (ν) from 100 mV/s to 200 mV/s

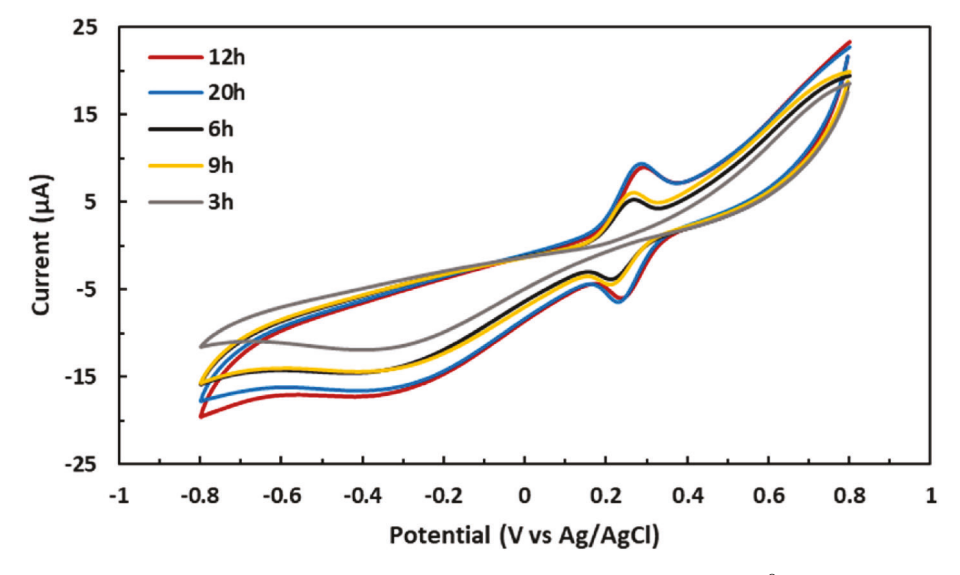


Fig. 4. Cyclic voltammograms indicating optimal incubation time of SARS-CoV-2 at 1.02×10^8 TCID50/mL concentration.

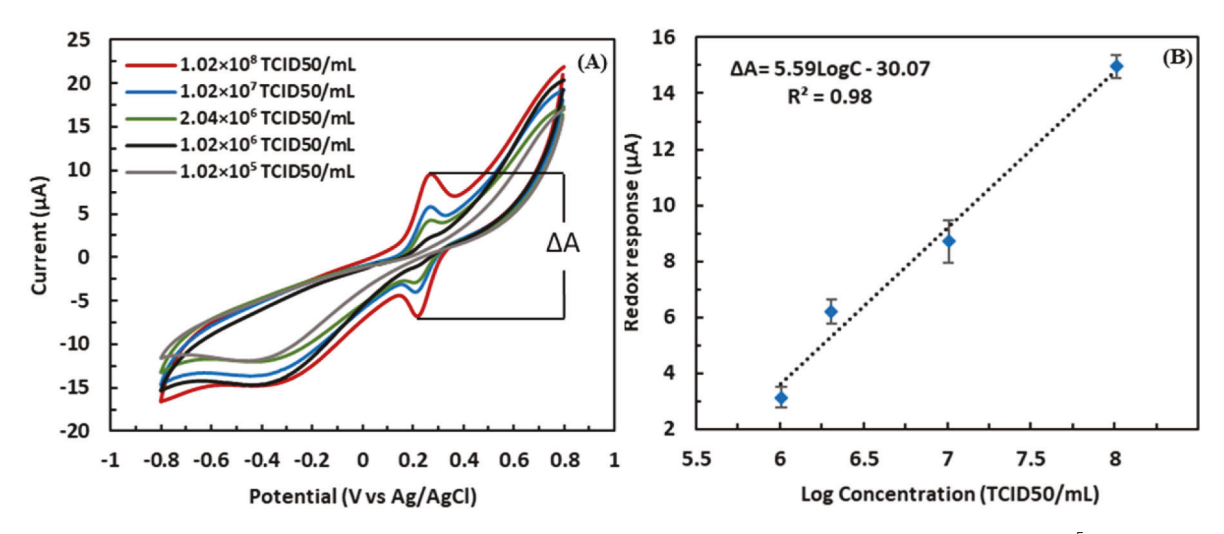


Fig. 5. (A) Cyclic Voltammograms showing variations in redox peaks for different concentrations of SARS-CoV-2 ranging from 1.02×10^5 TCID50/mL to 1.02×10^8 TCID50/mL. (B) Calibration curve displaying a linear relationship between redox response (ΔA) and log of virus concentration.

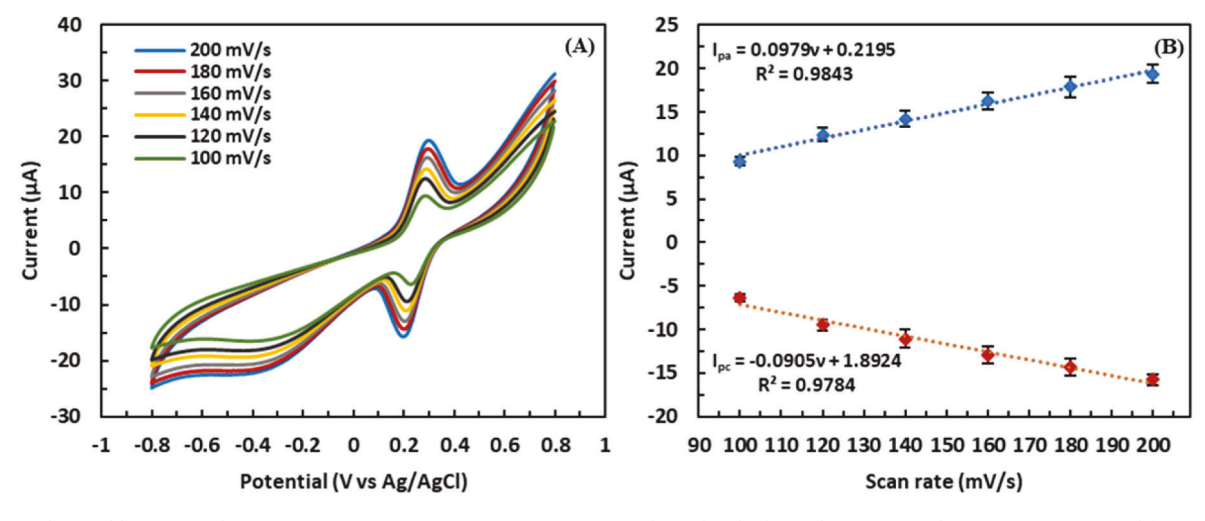


Fig. 6. Electrochemical kinetics analysis using CV measurements. (A) Variation in anodic and cathodic peak currents as the scan rate is increased from 100 mV/s to 200 mV/s. (B) Linear relationship between scan rate and peak current response, is indicative of a surface-controlled electrochemical process.

with steps of 20 mV/s during the CV analysis. As shown in Fig. 6A, an increase in the scan rate resulted in a corresponding gradual increase in both anodic and cathodic peak currents. This phenomenon can be attributed to the electrode having less time to achieve an equilibrium at each potential when the scan rate is increased. Consequently, the rate of electron transfer, which is directly proportional to the current, must increase to keep up with the increased rate of potential change, leading to higher peak currents [59]. The linear correlation between the scan rate and the peak current response of the sensor, as highlighted in Fig. 6B, implies that the electrochemical reaction taking place on the electrode surface is a traditional surface-controlled electrochemical process [60,61]. As depicted in Fig. 6A, a rise in the scan rate resulted in the cathodic peak potential moving to more negative values and the anodic peak potential to more positive values, leading to an expanded peak-to-peak separation. Furthermore, the change in anodic peak current (ΔI_{pa}) was not the same as the change in cathodic peak current (ΔI_{DC}) , suggesting that the redox reaction is quasi-reversible [62,63].

3.6. Selectivity of the biosensor

One of the paramount analytical characteristics of sensors is the selectivity toward a target analyte. To evaluate the selectivity of the proposed biosensor towards SARS-CoV-2, both CV and EIS analyses were carried out using H1N1, a subtype of influenza A virus, that may cause similar symptoms as SARS-CoV-2. It should be noted, however, that

while they may exhibit similarities in symptom presentation, the nuances in their structural components, like the spike proteins, can be distinct. Fig. 7 illustrates the redox responses of the biosensor to 1.02 \times 108 TCID50/mL of SARS-CoV-2 in contrast to H1N1 at a threefold greater concentration of 3×10^8 TCID50/mL. Remarkably, despite the higher concentration of H1N1, the biosensor exhibited a more pronounced redox response to SARS-CoV-2, demonstrating its high selectivity for SARS-CoV-2. Additionally, the EIS results, depicted in Fig. 7B, further validate the pronounced selectivity of the biosensor for SARS-CoV-2 over H1N1, with SARS-CoV-2 showing a lower R_{ct}. Importantly, the phase angle shifts from the Bode plot analysis provide further evidence of selectivity for SARS-CoV-2. Fig. 7C reveals the distinct patterns of phase angle shifts for SARS-CoV-2 compared to H1N1. Particularly, the phase angle shifts observed at specific frequencies provide clear evidence of the ability of the biosensor to differentiate between the two viruses. The phase angle shifts of interest for SARS-CoV-2 were found to be -20.2° at 12.4 Hz and -44.6° at 315.5 Hz. In contrast, the shifts for H1N1 were -25.7° at 7.9 Hz and -59° at 198.6 Hz. The distinction between the shifts for SARS-CoV-2 and H1N1 at these specific points is notable, highlights the efficiency of the biosensor in differentiating SARS-CoV-2 from other viruses.

4. Conclusion

Two different linkers, PFDT and aryl diazonium salt, were utilized

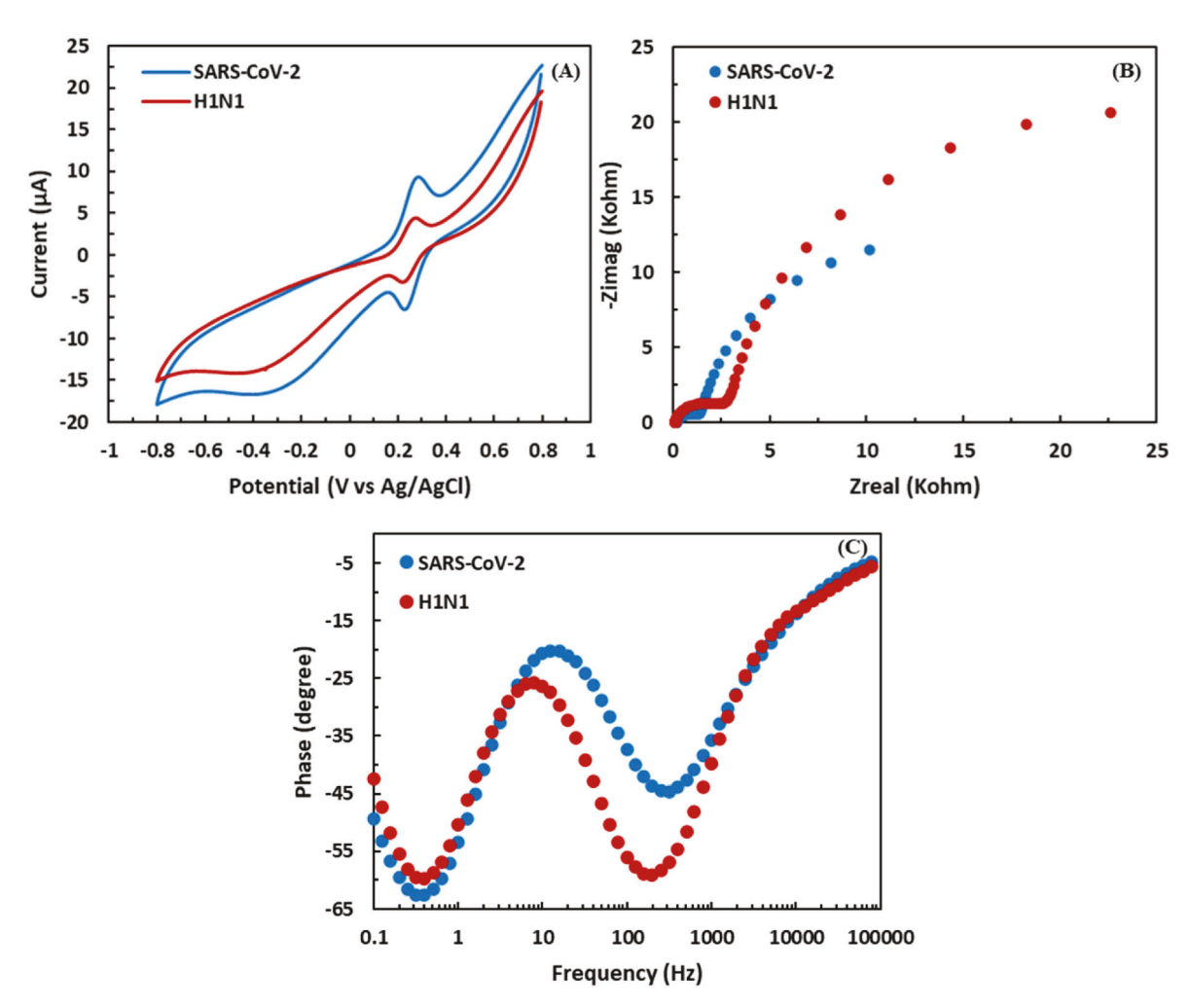


Fig. 7. Comparative analyses highlighting the selectivity of the proposed biosensor for SARS-CoV-2 over H1N1. (A) CV responses of the biosensor to SARS-CoV-2 at 1.02×10^8 TCID50/mL TCID50/mL and H1N1 at 3×10^8 TCID50/mL. Notably, despite the higher concentration of H1N1, the biosensor exhibits enhanced selectivity towards SARS-CoV-2. (B) Nyquist plots confirming the higher selectivity of the biosensor for SARS-CoV-2. (C) Phase angle shifts in Bode plots for SARS-CoV-2 and HIN1.

for the immobilization of the ACE2 enzyme on SPGEs and SPCEs, respectively. The propensity of fluorocarbons in PFDT to self-interact restricted its miscibility in organic solvents. As a result, electrodes modified with PFDT displayed recurrent inconsistencies. This inherent inconsistency adversely influenced both the immobilization of the ACE2 enzyme and the subsequent capture of SARS-CoV-2. It was also found that PFDT inhibited the redox functional groups of ACE2 from reacting with virus. In contrast, carbon electrodes modified with aryl diazonium exhibited consistent results, making it a more suitable linker for ACE2 enzyme immobilization. Both the binding of ACE2 on the aryl diazonium salt layer and the interaction between the bound ACE2 and virus were observed to increase the charge transfer rates. Using CV analysis, the optimal incubation time for SARS-CoV-2 was determined to be 12 h, as longer incubations resulted in no significant change due to saturation of the ACE2 enzyme with SARS-CoV-2. The biosensor exhibited a remarkable sensitivity, as shown by its notably low limit of detection (LOD: 1.02×10^6 TCID50/mL), and demonstrated a linear relationship between the redox response and the logarithm of SARS-CoV-2 concentration, ranging from 1.02×10^6 TCID50/mL to 1.02×10^8 TCID50/mL. The scan rate analysis demonstrated that the electrochemical reaction taking place on the electrode was governed by a surface-controlled electrochemical mechanism. Furthermore, the biosensor exhibited notable selectivity towards SARS-CoV-2, as shown by a more pronounced redox response compared to H1N1, even in the presence of H1N1 at a concentration three times higher. Acknowledging the potential areas for enhancement, our study recognizes certain limitations that pave the way for future research. While the sensor ensures accurate detection with a 12 h incubation period, further refinement to reduce this duration could enhance the practicality of the proposed sensor for more immediate diagnostic needs. In addition, while our findings confirm selectivity for SARS-CoV-2 over H1N1, yet the exploration of selectivity across a broader range of coronaviruses and potential interfering substances in clinical matrices remains a frontier for further investigation.

CRediT authorship contribution statement

Hamidreza Ghaedamini: Writing – original draft, Visualization, Validation, Software, Methodology, Investigation, Conceptualization. Khalid Khalaf: Writing – original draft, Software, Methodology, Data curation, Conceptualization. Dong-Shik Kim: Writing – review & editing, Validation, Supervision, Resources, Project administration, Investigation, Funding acquisition, Formal analysis, Conceptualization. Yuan Tang: Writing – review & editing, Validation, Supervision, Resources, Investigation, Funding acquisition, Formal analysis, Conceptualization.

Declaration of competing interest

The authors declare that they have no known competing financial interests or personal relationships that could have appeared to influence the work reported in this paper.

Data availability

Data will be made available on request.

Acknowledgements

The authors would like to acknowledge the support from the deArce-Koch Memorial Endowment Fund, NSF I-Corps (2323237) program, and the University of Toledo for providing the facilities and resources.

Appendix A. Supplementary data

Supplementary data to this article can be found online at https://doi. org/10.1016/j.ab.2024.115504.

References

- A. Georgas, et al., ACE2-based capacitance sensor for rapid native SARS-CoV-2 detection in biological fluids and its correlation with real-time PCR, Biosens. Bioelectron. 202 (2022) 114021.
- [2] C. Chaimayo, et al., Rapid SARS-CoV-2 antigen detection assay in comparison with real-time RT-PCR assay for laboratory diagnosis of COVID-19 in Thailand, Virol. J. 17 (2020) 1–7.
- [3] X. Ren, et al., Application and Optimization of RT-PCR in Diagnosis of SARS-CoV-2 Infection, MedRxiv, 2020, p. 2020, 02. 25.20027755.
- [4] M. Teymouri, et al., Recent advances and challenges of RT-PCR tests for the diagnosis of COVID-19, Pathol. Res. Pract. 221 (2021) 153443.
- [5] E. Morales-Narváez, C. Dincer, The impact of biosensing in a pandemic outbreak: COVID-19, Biosens. Bioelectron. 163 (2020) 112274.
- [6] B.S. Vadlamani, et al., Functionalized TiO2 nanotube-based electrochemical biosensor for rapid detection of SARS-CoV-2, Sensors 20 (20) (2020) 5871.
- [7] S. Imran, S. Ahmadi, K. Kerman, Electrochemical biosensors for the detection of SARS-CoV-2 and other viruses, Micromachines 12 (2) (2021) 174.
- [8] E. Cesewski, B.N. Johnson, Electrochemical biosensors for pathogen detection, Biosens. Bioelectron. 159 (2020) 112214.
- [9] M. Manzano, et al., Rapid and label-free electrochemical DNA biosensor for detecting hepatitis A virus, Biosens. Bioelectron. 100 (2018) 89–95.
- [10] P.M. Shaibani, et al., Metabolic study of cancer cells using a pH sensitive hydrogel nanofiber light addressable potentiometric sensor, ACS Sens. 2 (1) (2017) 151–156.
- [11] A. Butterworth, et al., SAM composition and electrode roughness affect performance of a DNA biosensor for antibiotic resistance, Biosensors 9 (1) (2019) 22
- [12] E.O. Blair, et al., Biologically modified microelectrode sensors provide enhanced sensitivity for detection of nucleic acid sequences from Mycobacterium tuberculosis, Sensors and Actuators Reports 2 (1) (2020) 100008.
- [13] N. Olgaç, Y. Şahin, L. Liv, Development and characterisation of cysteine-based gold electrodes for the electrochemical biosensing of the SARS-CoV-2 spike antigen, Analyst 147 (20) (2022) 4462–4472.
- [14] L. Liv, A. Baş, Discriminative electrochemical biosensing of wildtype and omicron variant of SARS-CoV-2 nucleocapsid protein with single platform, Anal. Biochem. 657 (2022) 114898.
- [15] L. Liv, H. Kayabay, An electrochemical biosensing platform for the SARS-CoV-2 spike antibody detection based on the functionalised sars-cov-2 spike antigen modified electrode, ChemistrySelect 7 (10) (2022) e202200256.
- [16] L. Liv, Electrochemical immunosensor platform based on gold-clusters, cysteamine and glutaraldehyde modified electrode for diagnosing COVID-19, Microchem. J. 168 (2021) 106445.
- [17] L. Liv, et al., Electrochemical biosensing platform based on hydrogen bonding for detection of the SARS-CoV-2 spike antibody, Anal. Bioanal. Chem. 414 (3) (2022) 1313–1322.
- [18] X. Zeng, Z. Shen, R. Mernaugh, Recombinant antibodies and their use in biosensors, Anal. Bioanal. Chem. 402 (2012) 3027–3038.
- [19] V. Vezza, et al., An Uncomplicated Electrochemical Sensor Combining a Perfluorocarbon SAM and ACE2 as the Bio-Recognition Element to Sensitively and Specifically Detect SARS-CoV-2 in Complex Samples, 2020.
- [20] C.W. Tan, et al., A SARS-CoV-2 surrogate virus neutralization test based on antibody-mediated blockage of ACE2-spike protein-protein interaction, Nat. Biotechnol. 38 (9) (2020) 1073–1078.
- [21] M.-Y. Li, et al., Expression of the SARS-CoV-2 cell receptor gene ACE2 in a wide variety of human tissues, Infectious diseases of poverty 9 (2) (2020) 23–29.
- [22] J. Zhang, et al., Progress and prospects on vaccine development against SARS-CoV-2, Vaccines 8 (2) (2020) 153.
- [23] M. Ejemel, et al., A cross-reactive human IgA monoclonal antibody blocks SARS-CoV-2 spike-ACE2 interaction, Nat. Commun. 11 (1) (2020) 4198.
- [24] J. Lan, et al., Structure of the SARS-CoV-2 spike receptor-binding domain bound to the ACE2 receptor, nature 581 (7807) (2020) 215–220.
- [25] Y. Xie, et al., Spike proteins of SARS-CoV and SARS-CoV-2 utilize different mechanisms to bind with human ACE2, Front. Mol. Biosci. 7 (2020) 392.
- [26] D. Clayton, et al., Structural determinants for binding to angiotensin converting enzyme 2 (ACE2) and angiotensin receptors 1 and 2, Front. Pharmacol. 6 (2015) 5.
- [27] Z. Yang, et al., Analytical application of self assembled monolayers on gold electrodes: critical importance of surface pretreatment, Biosens. Bioelectron. 10 (9–10) (1995) 789–795.
- [28] B.-W. Park, D.-Y. Yoon, D.-S. Kim, Formation and modification of a binary self-assembled monolayer on a nano-structured gold electrode and its structural characterization by electrochemical impedance spectroscopy, Journal of electroanalytical chemistry 661 (2) (2011) 329–335.
- [29] M. Gebala, W. Schuhmann, Controlled orientation of DNA in a binary SAM as a key for the successful determination of DNA hybridization by means of electrochemical impedance spectroscopy, ChemPhysChem 11 (13) (2010) 2887–2895.
- [30] J. Tkac, J.J. Davis, An optimised electrode pre-treatment for SAM formation on polycrystalline gold, J. Electroanal. Chem. 621 (1) (2008) 117–120.
- [31] S. Liebana, G.A. Drago, Bioconjugation and stabilisation of biomolecules in biosensors, Essays Biochem. 60 (1) (2016) 59–68.
- [32] G. Paimard, E. Ghasali, M. Baeza, Screen-printed electrodes: fabrication, modification, and biosensing applications, Chemosensors 11 (2) (2023) 113.
- [33] A.P. Washe, et al., Facile and versatile approaches to enhancing electrochemical performance of screen printed electrodes, Electrochim. Acta 91 (2013) 166–172.

- [34] S. Tajik, et al., High performance of screen-printed graphite electrode modified with Ni–Mo-MOF for voltammetric determination of amaranth, J. Food Meas. Char. 15 (2021) 4617–4622.
- [35] D. Antuña-Jiménez, et al., Screen-printed electrodes modified with metal nanoparticles for small molecule sensing, Biosensors 10 (2) (2020) 9.
- [36] F. Ricci, et al., Prussian Blue and enzyme bulk-modified screen-printed electrodes for hydrogen peroxide and glucose determination with improved storage and operational stability, Anal. Chim. Acta 485 (1) (2003) 111–120.
- [37] M. Rosal, et al., Dimethylglyoxime modified screen-printed electrodes for nickel determination, J. Electroanal. Chem. 839 (2019) 83–89.
- [38] F. Darain, S.-U. Park, Y.-B. Shim, Disposable amperometric immunosensor system for rabbit IgG using a conducting polymer modified screen-printed electrode, Biosens. Bioelectron. 18 (5–6) (2003) 773–780.
- [39] W. Yantasee, et al., Screen-printed electrodes modified with functionalized mesoporous silica for voltammetric analysis of toxic metal ions, Electrochem. Commun. 7 (11) (2005) 1170–1176.
- [40] V.J. Vezza, et al., An electrochemical SARS-CoV-2 biosensor inspired by glucose test strip manufacturing processes, Chem. Commun. 57 (30) (2021) 3704–3707.
- [41] P. Towler, et al., ACE2 X-ray structures reveal a large hinge-bending motion important for inhibitor binding and catalysis, J. Biol. Chem. 279 (17) (2004) 17996–18007.
- [42] H. Ghaedamini, et al., Reduced glutathione-modified electrode for the detection of hydroxyl free radicals, Biosensors 13 (2) (2023) 254.
- [43] C. Pérez-Ràfols, et al., A screen-printed voltammetric electronic tongue for the analysis of complex mixtures of metal ions, Sensor. Actuator. B Chem. 250 (2017) 393–401
- [44] J. Puy-Llovera, et al., Selenocystine modified screen-printed electrode as an alternative sensor for the voltammetric determination of metal ions, Talanta 175 (2017) 501–506.
- [45] A. Sharma, et al., Electrochemical impedance spectroscopy study of carbohydrate-terminated alkanethiol monolayers on nanoporous gold: implications for pore wetting, J. Electroanal. Chem. 782 (2016) 174–181.
- [46] K.A. Mahmoud, S. Hrapovic, J.H. Luong, Picomolar detection of protease using peptide/single walled carbon nanotube/gold nanoparticle-modified electrode, ACS Nano 2 (5) (2008) 1051–1057.
- [47] N.S. Heo, et al., Label-free electrochemical diagnosis of viral antigens with genetically engineered fusion protein, Sensors 12 (8) (2012) 10097–10108.
- [48] U. Jarocka, et al., An immunosensor based on antibody binding fragments attached to gold nanoparticles for the detection of peptides derived from avian influenza hemagglutinin H5, Sensors 14 (9) (2014) 15714–15728.

- [49] E. Ahlberg, B. Helgee, V.D. Parker, The reaction of aryl radicals with metallic electrodes, Acta Chem. Scand. B 34 (1980) 181–186.
- [50] W. Yang, Y. Li, Y. Feng, High electrochemical performance from oxygen functional groups containing porous activated carbon electrode of supercapacitors, Materials 11 (12) (2018) 2455
- [51] H. Radinger, A surface odyssey. Role of oxygen functional groups on activated carbon-based electrodes in vanadium flow batteries, ChemPhysChem 22 (24) (2021) 2498–2505, 2021.
- [52] E. Joonaki, et al., Surface chemistry can unlock drivers of surface stability of SARS-CoV-2 in a variety of environmental conditions, Chem 6 (9) (2020) 2135–2146.
- [53] M. Cametti, et al., The fluorous effect in biomolecular applications, Chem. Soc. Rev. 41 (1) (2012) 31–42.
- [54] G.E. Flynn, et al., Reversible DNA micro-patterning using the fluorous effect, Chem. Commun. 53 (21) (2017) 3094–3097.
- [55] J.A. Gladysz, D.P. Curran, I.T. Horváth, Handbook of Fluorous Chemistry, John Wiley & Sons, 2006.
- [56] M. Lock, et al., Sensitive determination of infectious titer of recombinant adenoassociated viruses (rAAVs) using TCID50 end-point dilution and quantitative polymerase chain reaction (qPCR), Cold Spring Harbor Protocols 2020 (5) (2020) pdb. prot095653.
- [57] H. Ghaedamini, A.C. Alba-Rubio, D.-S. Kim, A novel electrochemical sensor based on a cerium oxide/gold/carbon nanocomposite for the detection of hydroxyl free radicals, J. Electrochem. Soc. 170 (2023) 047510.
- [58] M. Mehmandoust, et al., Electrochemical immunosensor for rapid and highly sensitive detection of SARS-CoV-2 antigen in the nasal sample, Talanta 240 (2022) 123211.
- [59] Y. Denis, et al., Study of LiFePO4 by cyclic voltammetry, J. Electrochem. Soc. 154 (4) (2007) A253.
- [60] H. Liu, et al., A novel hydrogen peroxide biosensor based on immobilized hemoglobin in 3D flower-like MoS2 microspheres structure, Mater. Lett. 122 (2014) 182–185.
- [61] Y. Xu, et al., A novel electrochemical sensor for determination of hydroxyl radicals in living cells by coupling nanoporous gold layer with self-assembled 6-(Ferrocenyl) hexanethiol, Anal. Chim. Acta 1096 (2020) 69–75.
- [62] M. Arvand, R.M. Mazhabi, A. Niazi, Simultaneous determination of guanine, adenine and thymine using a modified carbon paste electrode by TiO2 nanoparticles-magnesium (II) doped natrolite zeolite, Electrochim. Acta 89 (2013) 669–679
- [63] X. Xu, et al., A novel amperometric hydrogen peroxide biosensor based on immobilized Hb in Pluronic P123-nanographene platelets composite, Colloids Surf. B Biointerfaces 84 (2) (2011) 427–432.